Supplementary material to: Randolph-Quinney PS, Williams SA, Steyn M, Meyer MR, Smilg JS, Churchill SE, et al. Osteogenic tumour in *Australopithecus sediba*: Earliest hominin evidence for neoplastic disease. S Afr J Sci. 2016;112(7/8), Art. #2015-0470, 7 pages. http://dx.doi.org/10.17159/sajs.2016/20150470

Differential diagnosis of U.W. 88-37

Table 1. Clinical and epidemiological characteristics: Primary and secondary differential diagnoses for U.W. 88-37 vertebral lesion

Disease	Pathological expression	Elements and regions affected	Prevalence (where known)
Osteoid osteoma (OO)	Benign painful tumour. Usually less than 20 mm diameter. Presents clinically as a nidus framed with a thin fibrovascular rim surrounded by sclerotic tissues of host bone. Radiologically seen as round or oval lesions less than 2 cm in diameter, with a 1–2 mm peripheral radiolucent zone in radiographs.	80% of cases found in the long bones. 5–10% of cases found in spine; of these 59% affect lumbar region, 27% cervical, 12% thoracic, and 2% sacrum.	Common. Accounts for over 12% of bone-forming tumours. Mainly affects individuals younger than 30 years. Male to female ratio 2.2:1.
Osteoblastoma (OB)	Also called giant osteoid osteoma. Benign bone-forming tumour; but can present with more aggressive characteristics than OO. Undergoes continuous remodelling and presents as sharply marginated structure with peripheral rind of sclerotic bone; in active cases trabeculae connect with the bony edge of the tumour. May present a nidus surrounded by radiolucent halo similar to OO; 25% of cases mimic a malignant growth.	30–36% of cases occur in the vertebral column; affects dorsal elements (lamina, pedicle, tranverse or spinous process).	Very rare; accounts for less than 1% of all bone-forming tumours. 80–90% of cases are seen in patients younger than 30 years. Male to female ratio 1.9:1
Giant cell tumour (GCT)	Benign tumour. Typically presents as large, diffuse and ill-defined osteolytic areas; lesions tend to be aggressive with multiple compartments. The characteristic radiological features include localised osteolysis with trabeculation in the long bone epiphysis, with metaphyseal extension after physeal fusion and ballooning in flat and irregular bones.	Most common at the end of long bones. The spine is involved in only 7% of cases. When GCT does affect spine, sacrum is usually involved, affecting 90% of cases.	Rare; accounts for 5% of all bone tumours. Most cases are found in adults between 30 and 40 years of age. Condition is slightly more common in women than men.
Aneurysmal bone cyst (ABC)	This is a spongy, multilocular, cystic lesion containing freely flowing blood or fluid. Arises as a consequence of primary bone tumours or trauma. Some aneurysmal cysts present with extensive periosteal new bone formation, whereas others are filled with new bone. Radiologically, ABC appears as a lytic, fluid-filled mass with well-defined smooth margins, often with cortical expansion, although the periosteum usually stays intact.	Can affect virtually any bone, but around 54% of cases are found in the long bones and 16% of cases affect spine. In vertebrae, it commonly affects the posterior elements and has a predilection for the thoracic region.	Rare; occurs in around 3% of biopsied bone tumours. 80% of cases occur under 20 years of age. Male to female ratio 2.5:1.
Enostosis	Not specifically a neoplasm. The lesion is composed of compact lamellar bone and expresses as ovoid, round or oblong in shape, measuring between 2 mm and 20 mm in diameter. When an enostosis occurs in a vertebra, it may have an osteoma-like appearance and is termed an endosteoma. Enostoses in the vertebrae are usually ivory-dense, and border but do not invade the endplate.	Can affect any bone. Specific regional incidence is unknown, but primarily affects the long bones, followed by pelvis and spine.	General incidence is unknown. Males and females are nearly equally affected.

Disease	Pathological expression	Elements and regions affected	Prevalence (where known)
Fibrous cortical defect (FCD)	Also known as fibroxanthoma or benign fibrous histiocytoma. Benign bony lesion is histologically identical to larger non-ossifying fibroma (NOF). Appear as small (< 20–30 mm) lucent defects within the cortex that become sclerotic as they heal. Radiographically, FCD presents as a longitudinally stretched lucent defect surrounded by a thin sclerotic rim in the metaphyses of the long bones.	Typically located in distal femur, proximal or distal tibia, and less frequently in upper limb. Very rare in vertebrae, with only 11 such cases having been reported worldwide by 2010.	Typically occur in children. One of the most common benign bony lesions; when combined with NOF, are seen in up to 30–40% of subadults. Male to female ratio 2:1.
Plasmacytoma (PM)	Plasmacytoma is a systemic malignant cancer. Typically presents as ill-defined osteolytic areas. Commonly leads to complete destruction of vertebra, including intrusion into contents of neural canal.	Has a predilection for the thoracic spine and can involve the posterior vertebral components.	PM is the most frequent primary tumour affecting the skeleton.
Eosinophilic granuloma (EO)	Also known as Langerhans-cell histiocytosis. Benign. Resembles an inflammatory process rather than neoplasm. Presents as single autoimmune tumour because of the overproduction of histiocytes. Solitary lesions typically have a broad zone of transition, with ill-defined borders, indicating aggressive growth.	Usually manifests in the thoracic spine; affects the centrum, leading to a collapse and flattening. May also occasionally appear on posterior vertebral components.	General incidence is unknown. Most frequently observed in children aged 5–15 years. Male to female ratio 2:1.
Hydatid cyst infection (HCI)	A parasitic infestation. One of the oldest worldwide human diseases known; caused by larval *Echinococcus granulosus* tapeworm. Spreads by drinking water or eating plants contaminated with faeces of carnivores. In vertebrae, it is characterised by multivesicular diffuse infiltration of cancellous bone, including corpus, pedicles and laminae. Common in thoracic region, but does not remain localised.	Frequency of skeletal involvement is rare, leading to bony changes in only 2% of cases. Of these, vertebral column is the most common site of expression – occurring in around 42% of skeletal cases.	The present and archaeological distribution of the disease is closely tied to the use of dogs for herding cattle and sheep. No age or sex bias is reported in clinical cases.

Source: *Data derived from listed references*[1-25]

Differential diagnosis of U.W. 88-37: Bayesian statistical parameters

To quantifiably assess the likelihood of the differential diagnosis between osteoid osteoma and osteoblastoma, we applied Bayes Theorem of conditional probability to differentiate between the two pathological conditions. The Bayesian approach assesses the likelihood of the incidence of a particular event. It enables the combination of objective probabilities, such as clinical data, and subjective probabilities (e.g. knowledge and experience of clinicians) to calculate these probability estimates.[26]

The statistical basis of Bayes Theorem is an understanding of the probability (P) of the occurrence of an event, or of a hypothesis (H) being true, given a particular set of evidence (E). In addition, the theorem uses influential background knowledge or information (*b*) that is available when the likelihood of H is considered.[27-31] We thus focus on the relationship between independent and non-independent events which influence the final outcome probability.[27-31] The P of H is referred to as *conditional probability*, which acknowledges that H is conditional or dependent on available evidence E. This calculation is usually denoted as $P(H \mid E)$, which can be read as 'the probability of event H, given evidence E'. The vertical bar separates the event on the left (whose probability is of interest) from events on the right (whose outcomes are known and may affect the probability of the event of interest). The vertical bar therefore means 'conditional on'. Furthermore, $P(H \mid E.b)$ represents the probability of H given E, taking into account relevant background information *b*. This is calculated as follows:

$$P(H \mid E.b) = \frac{P(H \mid b)P(E \mid H.b)}{P(H \mid b)P(E \mid H.b) + P(\neg H \mid b)P(E \mid \neg H.b)}$$

Where P(H) is the prior probability that H is true, and $P(\neg H)$ the prior probability that H is false. $P(E \mid H)$ and $P(E \mid \neg H)$ represent conditional or consequent probabilities given available evidence and background information. Based on clinical incidence data, we estimate the prior and consequent probabilities for the two pathological conditions of interest, as shown in Table S2.

Table S2. Bayes Theorem parameters for calculating relative probability estimates for primary and secondary differential diagnoses for U.W. 88-37 vertebral lesion

Probability function	**Osteoblastoma: clinical incidence**	**Osteoid osteoma: clinical incidence**
$P(H \mid b)$	0·01	0·12
$P(\neg H \mid b)$	0·99	0·88
$P(E \mid H.b)$	0·36	0·10
$P(E \mid \neg H.b)$	0·05	0·05
Relative Probability	*0·068*	*0·214*

The basis of our analysis starts from acceptance that the pathological condition H is caused by primary neoplastic disease of bone. Based on published epidemiological incidence data for osteoid osteoma[19-21] and osteoblastoma[19-25], we accept the prior probability that P(H | b) represents osteoblastoma (OB) as 1% (P = 0·01) and osteoid osteoma (OO) as 12% (P=0·12). Hence OB accounts for less than 1% of bone-forming tumours, whereas OO expresses in around 12% of clinical cases. P(¬H | b) represents the probability that P(H | b) is false. We next assume conditional probabilities [P(E | H.b)] based on the specific anatomical region where each condition manifests in the skeleton. In this case, we assume P=0.36 for osteoblastoma (up to 36% of cases of OB occur in the vertebral column) and P=0·1 for osteoid osteoma (up to 10% of OO cases occur in the region). A false likelihood probability of 5% (P=0·05) is accepted for each condition. On the basis of these prior and conditional probabilities of expression in the vertebral column (as opposed to elsewhere in the skeleton), we derive a conditional probability of 0·214 for the likelihood of osteoid osteoma, and 0·068 for osteoblastoma. This result indicates a 3·75-fold likelihood that osteoid osteoma rather than osteoblastoma is represented in the case under study.

Methods of image data acquisition and visualisation

The U.W. 88-37 vertebral specimen was imaged using propagation phase-contrast X-ray synchrotron microtomography, performed at the European Synchrotron Radiation Facility (ESRF) in Grenoble, France, on the beamline ID19. The imaging was done immediately after the complete imaging of the skull of MH1 performed on ID17.[32] This technique is today widely accepted as the gold standard for high quality 3D non-destructive imaging fossils.[33,34] The specimen was imaged in conjunction with a number of other anatomical elements from MH1 of similar size; the specimen was later cropped out from the combined plate to obtain an isolated volume.

Regarding the size and mineralisation level of the specimens, we used a high-energy polychromatic beam on the beamline ID19 of 55*10mm. To reach suitable effective energy, the white beam produced by the ID19 W150 wiggler with a gap closed at 60 mm was filtered with 3 mm of aluminium and 1 mm of copper, resulting in an average energy of 72 keV. The detector was a FreLoN 2K (Fast Readout Low Noise) CCD (charged couple device) camera[35], mounted on an optical system providing a final voxel size of 30.93 µm. This indirect detector was coupled with a 750-µm-thick LuAG:Ce (Lutetium Aluminium Garnet doped with Cerium) scintillator. When combining the polychromatic spectrum with the detector properties, the average detected energy was 76 keV (see source and detected spectrums). These parameters allow about 30% of minimum transmission through the specimens, with a reasonably small bandwidth (see Figure S3). The result is data that are nearly free of beam-hardening artefacts, but with a far faster acquisition speed than when using monochromatic beam and at a higher dynamical level. A propagation distance of

900 mm was used to obtain some phase-contrast effect, to enhance the visibility of the smallest structures and to increase the signal-to-noise ratio.

The plate with the different samples mounted was imaged using half-acquisition geometry (centre of rotation on one side of the field of view, coupled with 360° rotation) to increase the lateral field of view 1·8-fold relative to the normal view. Scans were performed using 4000 projections of 0·2 s each, over 360°, in continuous rotation mode. We used the frame transfer mode of the camera, which allows one to work without a physical shutter as long as the exposure time is greater than 0·1 s. Each scan lasted 21 min, and 24 scans were performed to image the full plate. The specimen was moved by half of the vertical field of view for each new scan, to ensure that each part of the fossils was imaged twice, using both the centre and border of the beam. This double-scanning approach, with suitable vertical concatenation, avoids the vertical power and spectral gradients from the wiggler source, ensuring constant dynamical level for the imaging of the whole specimen.

The radiographic data were then reconstructed using PyHST software (developed at ESRF). The reconstructions were based on filtered back-projection algorithms combined with a single distance phase retrieval process, adapted from Paganin and colleagues[36]. We applied the reconstruction protocol described by Sanchez and colleagues[37], by adding a 3D unsharp filter on the reconstructions after the phase retrieval process. This compensates for blurring introduced by the algorithm and allows retention of the higher sensitivity of phase retrieval process, without loss of the resolution from the edge detection effect. This approach can provide data similar to absorption contrast, as the specimens are relatively homogeneous regarding their chemical composition, but with a signal-to-noise ratio about 50 times better than real absorption scans, and a higher visibility of small details.[37] Finally, a light correction of ring artefacts was applied on reconstructed slices to ensure the highest possible quality of the final volume.

The 3D renderings and segmentation were performed using the software VGStudioMax 2·2 (Volume Graphics, Heidelberg, Germany). The rendering for solid views was performed with Phong's algorithm in volume rendering, with false colours attributed to different grey levels of tomographic data (dark brown for bone to light brown for matrix), and a projected shadow effect. Segmentation of the lesion was made in three steps. First, missing bone surface was recreated by a mirror image of the other side of the vertebra, to delineate the volume of lesion enclosed in the original bone shape. Then the empty cavity was segmented by simple region growing. Finally, a manual segmentation mask was performed for the area still filled with matrix, by careful delineation on one slice in every four. This first mask was then used to constrain a new region growing to segment only the matrix part, after which the bone was removed from the original segment. The final result was segmentation as close as possible to the real lesion surface, up to the detail levels. The 3D rendering of the lesion was then performed using false colours attributed to the grey levels (from red applied on air and matrix to light pink for voxels in direct contact with bones). Finally, a semi-transparent model of the complete vertebra with the lesion was prepared by selecting a 10-

voxel-thickness layer on the whole surface of the vertebra, set as transparent with Phong algorithm at 10%. (See Supplementary Figure S1.) All this imaging, data processing, segmentation and 3D rendering were performed by P.T.

Additional imaging of user-defined and oriented orthoslices was undertaken by P.S.R.Q. using Avizo Amira 5·4·5. Orthoslices were produced through secondary reconstruction of the image volume, with manipulation of orthogonal axes using the multi-planar viewer facility (see Supplementary Figure S2).

Additional medical imaging data

Figure S1: (a) vertebra U.W. 88-37.

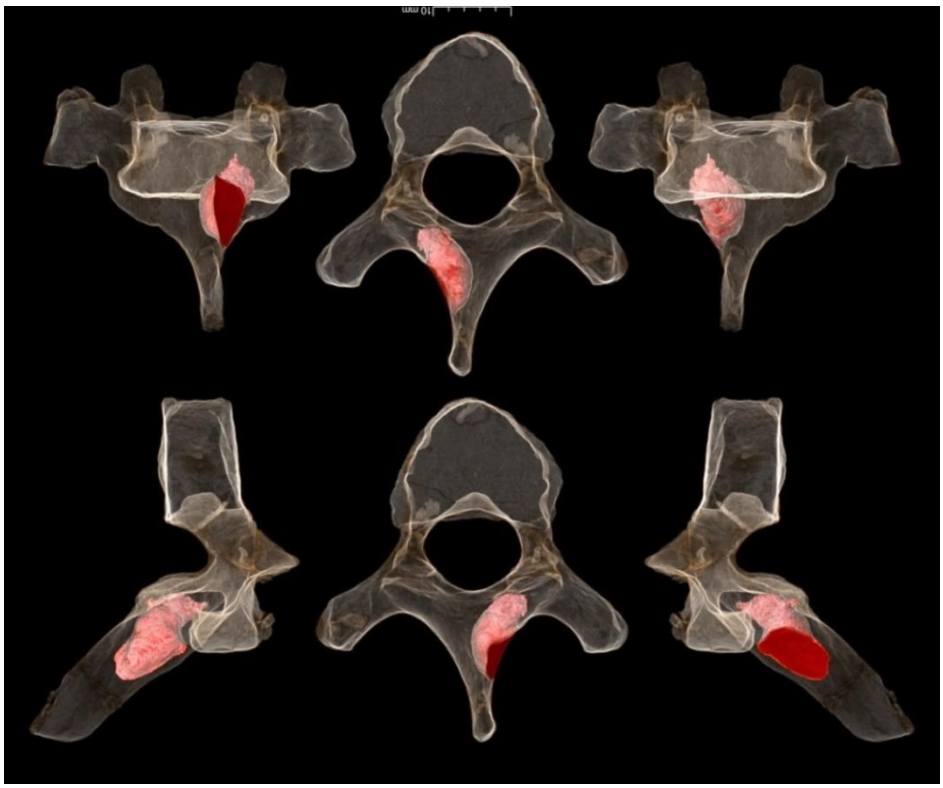

Figure S1: (b) additional images of surface-rendered image volume.

Images produced by P.T.

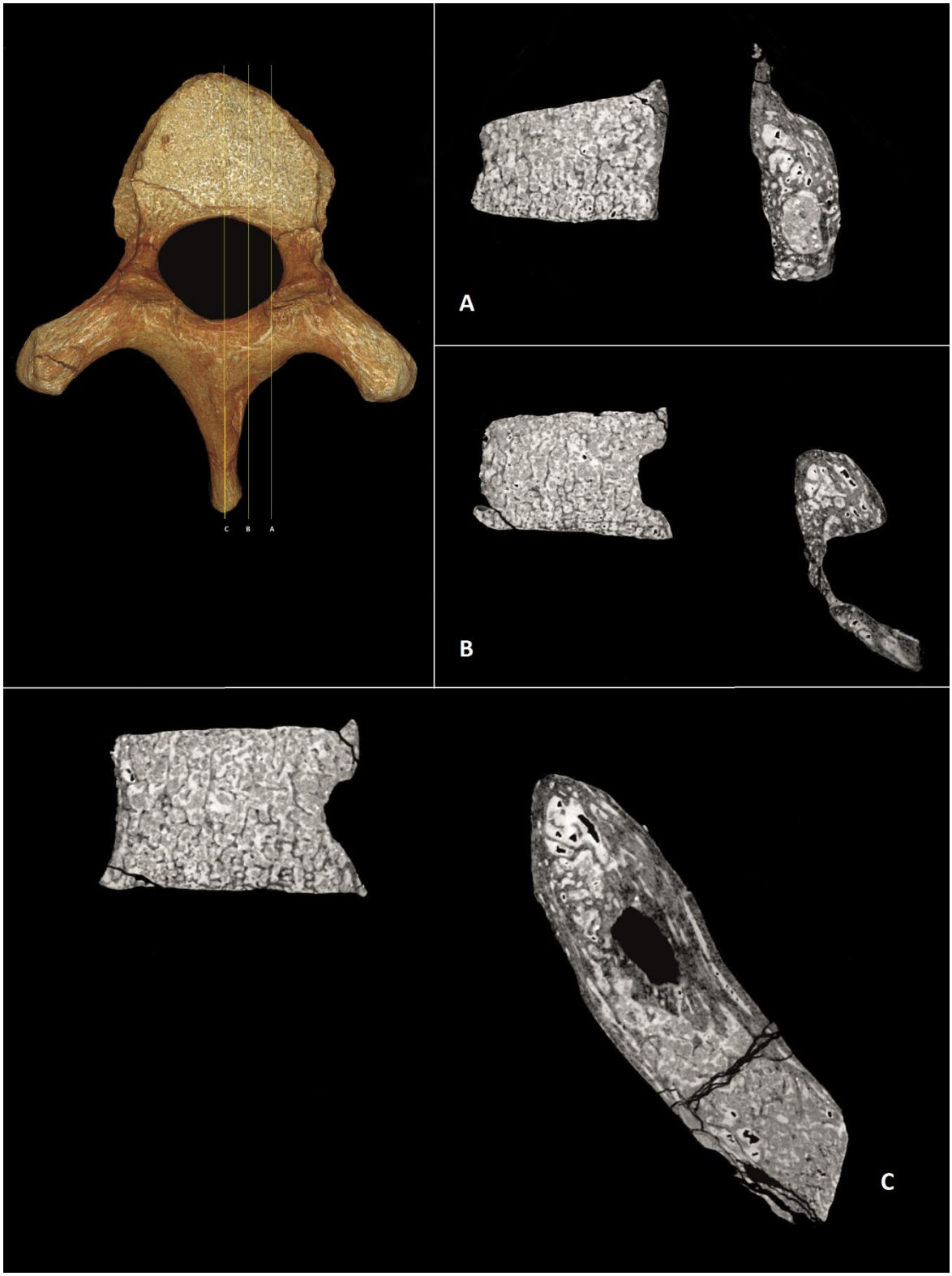

Figure S2: Sagittal slices through vertebra U.W. 88-37 derived from phase-contrast X-ray synchrotron microtomography. Relative position and anatomical orientation of orthoslices A, B and C are shown on the volume-rendered model. The posterior portion is sclerotic, with circumscribed margins of well-integrated cortical bone, abutted and intersected by trabecular striae, with remodelling and reorganisation of the cortex. The anterior portion of the lesion displays a geographic pattern of bone destruction, showing a sharp non-sclerotic margin and evidence of active osteolytic processes, with sharply defined transection of individual trabeculae, and active osteolytic penetration into the anterior portion of the lamina. Images produced by P.S.R.Q.

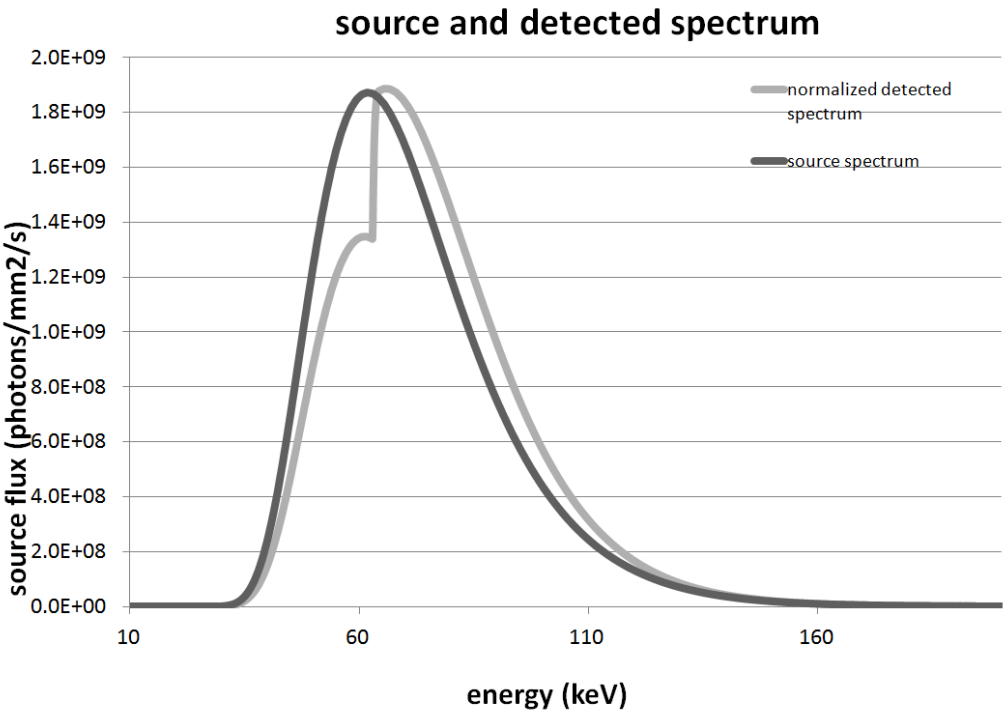

Figure S3: Source and detected spectrum for imaging of U.W. 88-37 conducted on beamline ID19

References

1. Ortner DJ. Tumors and tumor-like lesions of bone. In: Ortner DJ, editor. Identification of pathological conditions in human skeletal remains. Amsterdam: Academic Press; 2003. p. 503–544. http://dx.doi.org/10.1016/B978-012528628-2/50057-0
2. Bahk Y-W. Combined scintigraphic and radiographic diagnosis of bone and joint diseases. New York: Springer; 2007. http://dx.doi.org/10.1007/978-3-540-68732-0_4
3. Khurana JS. The surgical pathology of bone tumors and tumor-like lesions. In: Khurana JS, editor. Bone pathology. London: Humana Press; 2009. p. 285–345. http://dx.doi.org/10.1007/978-1-59745-347-9_19
4. McCall IW. Radiology and pathological correlations of bone tumours of the spine. In: Gourtsoyiannis NC, Ros PR, editors. Radiologic-pathologic correlations from head to toe: Understanding the manifestations of disease. Berlin: Springer; 2005. p. 721–742. http://dx.doi.org/10.1007/3-540-26664-X_32
5. Vigorita VJ. Orthopaedic pathology. 2nd ed. Philadelphia: Lippincott Williams & Wilkins; 2008.
6. Baba H, Maezawa Y, Furusawa N, Wada M, Kokubo Y, Imura S, et al. Solitary plasmacytomas of the spine associated with neurological complications. Spinal Cord. 1998;36(7):470–475. http://dx.doi.org/10.1038/sj.sc.3100572
7. Berry M, Mankin H, Gebhardt M, Rosenberg A, Hornicek F. Osteoblastoma: A 30-year study of 99 Cases. J Surg Oncol. 2008;98:179–183. http://dx.doi.org/10.1002/jso.21105
8. Betsy M, Kupersmith LM, Springfield DS. Metaphyseal fibrous defects. J Am Acad Orthop Surg. 2004;12(2):89–95. http://dx.doi.org/10.5435/00124635-200403000-00004
9. Binning M, Klimo Jr P, Gluf W, Goumnerova L. Spinal tumors in children. Neurosurg Clin N Am. 2007;18(4):631–658. http://dx.doi.org/10.1016/j.nec.2007.07.001

10. McLain RF, Weinstein JN. Solitary plasmacytomas of the spine: A review of 84 cases. J Spinal Disord. 1989;2(2):69–74. http://dx.doi.org/10.1097/00002517-198906000-00001

11. Mendenhall WM, Zlotecki RA, Scarborough MT, Gibbs CP, Mendenhall NP. Giant cell tumor of bone. Am J Clin Oncol. 2006;29(1):96–99. http://dx.doi.org/10.1097/01.coc.0000195089.11620.b7

12. Celik C, Münevver FS, Ucan H. Spinal hydatid cyst: Review. Türkiye Klinikleri J Med Sci. 2010;30(3):1073–1077. http://dx.doi.org/10.5336/medsci.2009-13722

13. Kransdorf MJ, Sweet DE. Aneurysmal bone cyst: Concept, controversy, clinical presentation, and imaging. Am J Roentgenol. 1995;164(3):573–580. http://dx.doi.org/10.2214/ajr.164.3.7863874

14. Osborn AG. Tumors, cysts, and tumorlike lesions of the spine and spinal cord. In: Osborn AG, editor. Diagnostic neuroradiology. St. Louis: Mosby; 1994. p. 876–918.

15. Kuruvath S, O'Donovan DG, Aspoas AR, David KM. Benign fibrous histiocytoma of the thoracic spine: Case report and review of the literature. J Neurosurg Spine. 2006;4(3):260–264. http://dx.doi.org/10.3171/spi.2006.4.3.260

16. Kaye JJ, Freiberger RH. Eosinophilic granuloma of the spine without vertebra plana: A report of two unusual cases. Radiology. 1969;92(6):1188–1191. http://dx.doi.org/10.1148/92.6.1188

17. Aufderheide AC, Rodríguez-Martin C. The Cambridge encylopedia of human paleopathology. Cambridge: Cambridge University Press; 1998.

18. Kan P, Schmidt MH. Osteoid osteoma and osteoblastoma of the spine. Neurosurg Clin North Am. 2008;19(1):65–70. http://dx.doi.org/10.1016/j.nec.2007.09.003

19. de Souza Dias L, Frost HM. Osteoid Osteoma–Osteoblastoma. Cancer. 1974;33(4):1075–1081. http://dx.doi.org/10.1002/1097-0142(197404)33:4<1075::AID-CNCR2820330427>3.0.CO;2-4

20. Azouz EM, Kozlowski K, Marton D, Sprague P, Zerhouni A, Asselah F. Osteoid osteoma and osteoblastoma of the spine in children: Report of 22 cases with brief literature review. Pediatr Radiol. 1986;16(1):25–31. http://dx.doi.org/10.1007/BF02387501

21. Saccomanni B. Osteoid osteoma and osteoblastoma of the spine: A review of the literature. Curr Rev Musculoskelet Med. 2009;2(1):65–67. http://dx.doi.org/10.1007/s12178-009-9047-6

22. Lucas DR. Osteoblastoma. Arch Pathol Lab Med. 2010;134:1460–1466.

23. Amacher AL, Eltomey A. Spinal osteoblastoma in children and adolescents. Child Nerv Syst. 1985;1(1):29–32. http://dx.doi.org/10.1007/BF00706727

24. Aszódi K. Benign osteoblastoma: Quantitative histological distinction from osteoid osteoma. Arch Orthop Unfallchir. 1977;88(3):359–368. http://dx.doi.org/10.1007/BF00416625

25. Boriani S, Capanna R, Donati D, Levine A, Picci P, Savini R. Osteoblastoma of the spine. Clin Orthop Relat Res. 1992;278:37–45. http://dx.doi.org/10.1097/00003086-199205000-00006

26. Lucy, D. Introduction to statistics for forensic scientists. London: Wiley; 2005.

27. Byers SN, Roberts CA. Bayes' theorem in paleopathological diagnosis. Am. J. Phys. Anthropol. 2003;121:1–9. http://dx.doi.org/10.1002/ajpa.10164

28. Evett IW. Bayesian-inference and forensic-science – Problems and perspectives. Statistician. 1987;36:99–105. http://dx.doi.org/10.2307/2348502

29. Taroni F, Aitken CGG. Probabilistic reasoning in the law – Part 1: Assessment of probabilities and explanation of the value of DNA evidence. Sci. Justice. 1998;38:165–177. http://dx.doi.org/10.1016/S1355-0306(98)72101-X

30. Taroni F, Aitken CGG. Probabilistic reasoning in the law – Part 2: Assessment of probabilities and explanation of the value of trace evidence other than DNA. Sci. Justice. 1998;38:179–188. http://dx.doi.org/10.1016/S1355-0306(98)72102-1

31. Taroni F, Bozza S, Aitken C. Decision analysis in forensic science. J. Forensic Sci. 2005;50:894–905. http://dx.doi.org/10.1520/JFS2004443

32. Carlson KJ, Stout D, Jashashvili T, de Ruiter DJ, Tafforeau P, Carlson K, Berger LR.The endocast of MH1, Australopithecus sediba. Science. 2011;333:1402–1407. http://dx.doi.org/10.1126/science.1203922

33. Tafforeau P, Hublin JJ, Smith TM. Hominin dental structure and development revealed non-destructively by multi-scale synchrotron imaging. Am J Phys Anthropol. 2009:252–252.

34. Tafforeau P, Boistel R, Boller E, Bravin A, Brunet M, Chaimanee Y, et al. Applications of X-ray synchrotron microtomography for non-destructive 3D studies of paleontological specimens. Appl Phys A-Mater. 2006;83:195–202. http://dx.doi.org/10.1007/s00339-006-3507-2

35. Labiche J-C, Mathon O, Pascarelli S, Newton MA, Ferre GG, Curfs C, et al. Invited article: The fast readout low noise camera as a versatile x-ray detector for time resolved dispersive extended x-ray absorption fine structure and diffraction studies of dynamic problems in materials science, chemistry, and catalysis. Rev Sci Instrum. 2007;78, Art. #091301. http://dx.doi.org/10.1063/1.2783112

36. Paganin D, Mayo S, Gureyev T, Miller P, Wilkins S. Simultaneous phase and amplitude extraction from a single defocused image of a homogeneous object. J Microsc Oxford. 2002;206:33–40. http://dx.doi.org/10.1046/j.1365-2818.2002.01010.x

37. Sanchez S, Ahlberg P, Trinajstic K, Mirone A, Tafforeau P. Three-dimensional synchrotron virtual paleohistology: A new insight into the world of fossil bone microstructures. Microsc Microanal. 2012;18:1095–1105. http://dx.doi.org/10.1017/S1431927612001079